Applied Physics Letters

Controlling length-scales of the phase separation to optimize organic semiconductor blends

Cite as: Appl. Phys. Lett. **107**, 201903 (2015); https://doi.org/10.1063/1.4935545
Submitted: 29 August 2015 . Accepted: 27 October 2015 . Published Online: 17 November 2015

C. Lorch, H. Frank, R. Banerjee, A. Hinderhofer, A. Gerlach, G. Li Destri, and F. Schreiber

Controlling length-scales of the phase separation to optimize organic semiconductor blends

C. Lorch,[1] H. Frank,[1] R. Banerjee,[1,2] A. Hinderhofer,[1] A. Gerlach,[1,a)] G. Li Destri,[3] and F. Schreiber[1]
[1]*Universität Tübingen, Institut für Angewandte Physik, Auf der Morgenstelle 10, 72076 Tübingen, Germany*
[2]*Department of Physics, Indian Institute of Technology Gandhinagar, Ahmedabad 382424, India*
[3]*ESRF-The European Synchrotron, 71 Avenue des Martyrs, 38000 Grenoble, France*

(Received 29 August 2015; accepted 27 October 2015; published online 17 November 2015)

The length-scale of phase separation in organic semiconductor donor-acceptor mixtures, while being crucially important for applications, is a non-trivial parameter to control in non-equilibrium thin film growth. We present a comprehensive study of all the important parameters that can be used to tailor the length-scale of phase separation in organic semiconductor mixtures. We employed different substrate temperatures, different growth rates, time-dependent deposition rates, and surface functionalization layers. We found not only that the substrate temperature is most prominent in influencing the length-scale of phase separation in the studied parameter range, but also that other routes can be used to tailor this length-scale. © *2015 AIP Publishing LLC*.
[http://dx.doi.org/10.1063/1.4935545]

Thin-film growth is fundamentally a non-equilibrium process, since achieving equilibrium is permanently disturbed by incoming material and energy.[1,2] Even for growth of single-compound films, small changes in the preparation conditions, such as deposition rate, substrate temperature, or substrate-adsorbate interaction, can lead to significantly different film structures and morphologies.[3] For mixtures of two (or more) compounds, the picture is even more complex. There are at least three idealised cases of how two materials may intermix: (a) solid solution—a stochastic mix of the two materials forms, (b) ordered complex—two materials show a mixed phase with periodic long-range order, and (c) phase separation—two ingredients tend to form separated domains of their pristine phases. The resulting mixing scenario depends on several parameters—*inter alia* the interaction energies between the different species, on the sterical compatibility in the case of molecules, and also on the preparation conditions like substrate temperature (T_{sub}), and/or deposition rate (r_{dep}).[4–8]

Mixtures of two organic compounds are often used in organic electronics, especially in organic photovoltaic (OPV) cells. Regarding the efficiency of the latter, it has been demonstrated that the length-scale of phase separation (l_s) of the electron donating and electron accepting material is crucially important, particularly in comparison to the length-scales of the electronic processes (i.e., exciton diffusion length) of the system.[9] On the one hand, if l_s is too small, free charge carriers might be trapped and their extraction hindered. On the other hand, if l_s is too large, excitons might not reach the donor-acceptor interface, which is necessary for the charge separation. If l_s is even larger, electrical short circuits may occur. From these considerations, one can conclude that the efficiency of OPV cells peaks for a certain l_s. This work is devoted to different ways of tailoring l_s, which can lead to improved efficiency of OPV cells.

OPV cells comprising the donor-acceptor combination of diindenoperylene (DIP) and buckminster fullerene (C_{60}) have been reported to have excellent values for the solar cell parameters, in particular, an extraordinarily high fill factor.[10] Furthermore, kinetically limited delayed phase separation has been reported to occur, keeping in mind the sterical incompatibility of the molecules.[11] DIP itself has a high exciton diffusion length,[12] exhibits ambipolar transport properties,[13] and its structural and morphological properties have been extensively studied.[14–18] C_{60} is a commonly used acceptor material in OPV cells.[19–21] The two materials together form a prototypical system of phase-separating mixtures; this offers the opportunity for a detailed understanding of the fundamental aspects of such material pairs, in general.

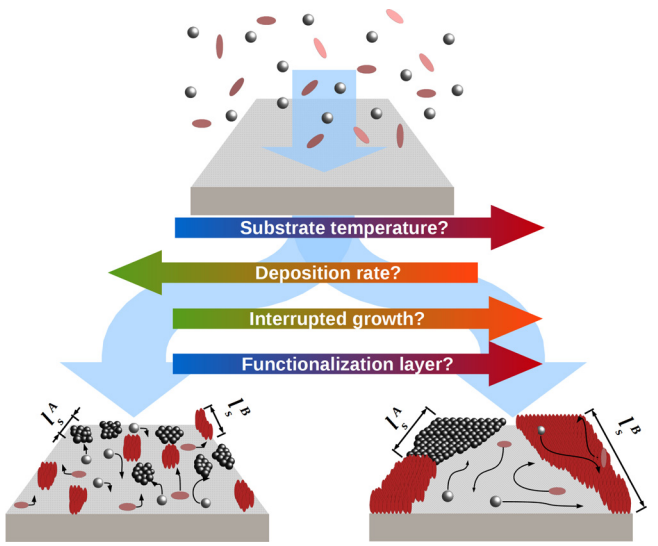

FIG. 1. Schematic of kinetically limited phase separation in a molecular mixture with length-scales of phase separation (l_s) for both materials A (l_s^A) and B (l_s^B). A high (low) substrate temperature, a low (high) deposition rate, interrupted (continuous) growth, or a functionalization layer (bare substrate) can be used to increase (decrease) the length-scale of phase separation.

a)Electronic mail: alexander.gerlach@uni-tuebingen.de

In bilayer geometry, where C_{60} is prepared on top of the DIP, a strong templating effect of the DIP, which improves its crystal structure significantly, has been reported.[22]

Here, we compare different routes to engineer the length-scale of the phase-separation in DIP:C_{60} mixed thin films prepared via organic molecular beam deposition. Fig. 1 depicts the various control parameters, which can be used for tailoring the phase-separation length-scale (l_s). In the conventional approach, the growth mainly depends on the ratio of the diffusion rate of the molecules $D(T)$ to the incoming flux of molecules (i.e., the deposition rate r_{dep}).[1] However, further methods can be used, such as a time-dependent deposition rate, as in interrupted growth, or surface functionalization. The bottom left-hand-side of Fig. 1 depicts low $D(T)$ and a high flux of incoming molecules, leading to a short length-scale when phase separating, whereas on the bottom right-hand-side, relatively high $D(T)$ and a small effective incoming flux lead to relatively large domains and, hence, a larger length-scale of phase-separation. We studied systematically the influence of all of the experimental parameters described above; the details of which are listed further below.

The films were characterised by *in situ* X-ray diffraction experiments, namely, X-ray reflectivity (XRR) and grazing incidence X-ray diffraction (GIXD). The roughness was extracted from the XRR data and GIXD, provided the averaged coherently scattering in-plane domain size $D_{coh\|}$, which is used as a gauge for the phase separation length-scale l_s.

Sublimation-grade DIP was obtained from the University of Stuttgart and C_{60} was purchased from Creaphys. The organic films were prepared via organic molecular beam deposition and investigated directly in a portable ultra-high vacuum chamber.[23] Native silicon oxide (nSiO) (oxide layer thickness $\sim$2 nm) was used as a substrate. The pressure in the vacuum chamber was less than 2×10^{-9} mbar during the deposition. The preparation parameters were varied for different samples, including the substrate temperature T_{sub}, the deposition rate r_{dep}, and the surface energy of the substrate, by applying a thin organic (DIP or C_{60}) layer. The deposition rates were controlled with a quartz crystal microbalance (QCM), which was calibrated via XRR.[24] The X-ray characterisation was performed at the ID10 beamline of the ESRF, with an energy of 14.0 keV (wavelength $\lambda = 0.886$ Å). The critical angle of the samples at this energy was 0.13°, and an incident angle of 0.1° was used for the GIXD scans. The XRR data were fitted using Parratt's formalism[25] with GenX[26] up to q_z-values of 0.2 $Å^{-1}$ for a quantitative analysis of the film roughness. The Bragg peaks of the GIXD data were fitted with Gaussian profiles, and Scherrer's formula was used to calculate the coherently scattering in-plane domain size $D_{coh\|} = 2\pi \cdot 0.94/FWHM$, where 0.94 is Scherrer's constant for spherical-like particles and $FWHM$ is the full-width at half-maximum of the fitted peak.[27] No broadening due to the experimental setup was included in the fit; hence, the values reported here represent lower limits for $D_{coh\|}$.

Methods for tailoring the length-scale of phase separation. The four different methods sketched in Fig. 1 were employed to tailor the length-scale of phase separation for DIP:C_{60} 1:1 mixtures. A nominal thickness of 20 nm was anticipated for all films. Table I lists the various parameters employed for the film growth. Three different T_{sub} (243 K, 303 K, and 373 K) were studied to vary the diffusion length $D(T)$ of the molecules on the substrate. Furthermore, the deposition rate r_{dep} was varied. At low r_{dep} ($r_{dep}^{low} = 0.15$ nm/min), the probability that molecules can form a new domain before attaching to an existing one is much lower as compared to the high r_{dep} ($r_{dep}^{high} = 1.2 - 1.4$ nm/min). Another way to vary the growth is to interrupt the growth in a systematic manner.[28] We allowed different growth and interruption times for both the low and high rates. At r_{dep}^{low}, we deposited for 400 s, which corresponds to depositing 1 nm followed by a break of 120 s. This deposition-break cycle was repeated 20 times in total in order to reach a nominal film thickness of 20 nm. Molecules were evaporated for 75 s, followed by the flux being interrupted for 75 s, in the case of r_{dep}^{high}. The deposited material amounted to 1.5 nm per cycle. The procedure was repeated up to a total thickness of 20 nm. One additional method to change the diffusion length is to change the substrate potential by employing either a monolayer of DIP or a thin C_{60} layer before co-deposition of both the materials. The resulting film architecture resembles a so-called planar mixed heterojunction, which, with the same material combination, has already been successfully employed for OPV devices.[29]

TABLE I. Different deposition strategies for the preparation of DIP:C_{60} (1:1) mixtures investigated in this study. The preparation of the templating layers are described in the text. The evaporation rates marked with * are the rates employed during the open shutter for growth runs with non-continuous rate. The thicknesses d and roughnesses σ (error for both is ±0.1 nm) were determined from XRR. The in-plane coherent crystal size $D_{coh\|}$ is averaged over several reflections and calculated via Scherrer's formula (error for each is ±0.3 nm). The values in the bottom row (temp. DIP) correspond to the pure DIP template.

T_{sub} (K)	Template	r_{dep} (nm/min)	Int.	d (nm)	σ (nm)	$D_{coh\|}$ C_{60} (nm)	$D_{coh\|}$ DIP (nm)
243	No	0.15	No	18.3	2.3	3.3	n.a.
243	DIP	0.15	No	18.0	0.6	3.2	n.a.
303	No	0.15	No	17.9	3.3	3.3	n.a.
303	DIP	0.15	No	16.9	2.8	3.0	11.3
303	C_{60}	0.15	No	19.0	2.8	3.6	4.5
303	No	0.15*	400/120	19.2	3.6	3.2	n.a.
303	No	1.20	No	19.6	2.4	n.a.	3.5
303	No	1.20*	75/75	20.0	2.9	3.3	6.4
373	No	0.15	No	20.8	5.5	7.5	35.5
373	DIP	0.15	No	21.2	5.1	8.0	47.4
373	No	1.42	No	22.6	5.0	8.4	11.9
303	Temp. DIP	0.15	n.a.	n.a.	n.a.	n.a.	6.9

Changing the substrate temperature. The XRR and GIXD data for the different T_{sub} are depicted in Figs. 2(a) and 2(b), respectively.[24]

Considering the out-of-plane data (Fig. 2(a)), all peaks can be associated either with standing-up DIP[15] or with the fcc C_{60} structural phase.[30] No additional peaks are observed, indicating that the materials phase-separate, and no new crystal structure is formed. In general, C_{60} crystallites on SiO_2 are oriented randomly with no preferred out-of-plane order.[22] With increasing substrate temperature, the out-of-plane crystallinity of the DIP improves, as evidenced by the enhanced DIP (0 0 1) and (0 0 2) Bragg peaks at $q_z = 0.37\,\text{Å}^{-1}$ and $q_z = 0.74\,\text{Å}^{-1}$. Another obvious trend is the increase of surface roughness (σ) with increasing substrate temperature, which can be concluded from the damping of the Kiessig oscillations in the low q_z region.[31] The extracted thicknesses and σ are summarized in Table I. The evolution of σ from 2.3 nm to 5.5 nm with increasing temperature is depicted in Fig. 2(c).

The results of the GIXD measurements are shown in Fig. 2(b). As seen in the out-of-plane data as well, only Bragg peaks associated with either standing-up DIP or the fcc structure of C_{60} appear. Generally speaking, the crystallinity of the films increases with increasing T_{sub}, visible in the sharper Bragg reflections at higher T_{sub}. The values extracted from the GIXD data are listed in Table I and visualized in Fig. 2(c–I). At $T_{sub} = 243$ and 303 K, only the C_{60} (1 1 1) peak can be distinguished clearly. The other Bragg peaks are buried under a wide hump in the $q_{xy} = 1.0$–$1.8\,\text{Å}^{-1}$ range, indicating that no large crystallites of any of the two materials are formed. Further increasing T_{sub} to 373 K, $D_{coh\|}$ of C_{60} and DIP increases from 3.3 to 7.5 nm and to 35.5 nm, respectively. Interestingly, at $T_{sub} = 373$ K, two additional peaks at $q_{xy} = 1.21\,\text{Å}^{-1}$ and $1.76\,\text{Å}^{-1}$ are observed. These two peaks can be associated with domains of an ordered DIP polymorph, already observed in pure DIP films.[32] $D_{coh\|}$ of these two peaks are 23.5 nm and 16.8 nm, respectively. These peaks are not observed for any of the other films.

Changing the deposition rate. The film prepared at 303 K with r_{dep}^{high} shows a slightly better out-of-plane crystal structure than the low-deposition-rate film. Additionally, this film is the one with the smallest surface roughness at $T_{sub} = 303$ K. In contrast to the out-of-plane data, the in-plane data of the high-rate film show only weak peaks corresponding to DIP and no C_{60} features at all. The latter is quite surprising since all other films show at least a broad Bragg peak corresponding to the C_{60} (1 1 1) orientation. However, at $T_{sub} = 373$ K, increasing r_{dep} by one order of magnitude influences strongly the in-plane structure: $D_{coh\|}$ of DIP decreases from 35.5 nm to 11.9 nm. For C_{60}, $D_{coh\|}$ is slightly higher (from 7.5 nm to 8.4 nm) (Fig. 2(c) **II**). The latter might be due to small variations in the mixing ratio, which might vary slightly over the preparation process.

Time-dependent deposition rate. There is basically no difference in the out-of-plane structure observed for the interrupted growth and the normal growth, at r_{dep}^{low}. Also, the in-plane structure is very similar in both cases (Fig. 2(c) **III**, left hand side). However, interrupted growth at r_{dep}^{high}, leads to a slightly better ordered film in the out-of-plane direction compared to the continuous growth with the same deposition rate. In addition, σ is slightly higher (2.4 nm vs. 2.9 nm) for the interrupted growth. The changes are more significant for the in-plane structure. Interrupting the growth causes $D_{coh\|}$ of DIP to increase to 6.4 nm (from 3.5 nm) and $D_{coh\|}$ of C_{60} to 3.3 nm, respectively, whereas, the latter cannot be determined at r_{dep}^{high} without interruptions (Fig. 2(c) **III**, right hand side).

Functionalization of the substrate. The DIP layer was employed at three different T_{sub}—243 K, 303 K, and 373 K—whereas, that of C_{60} was used only at 303 K

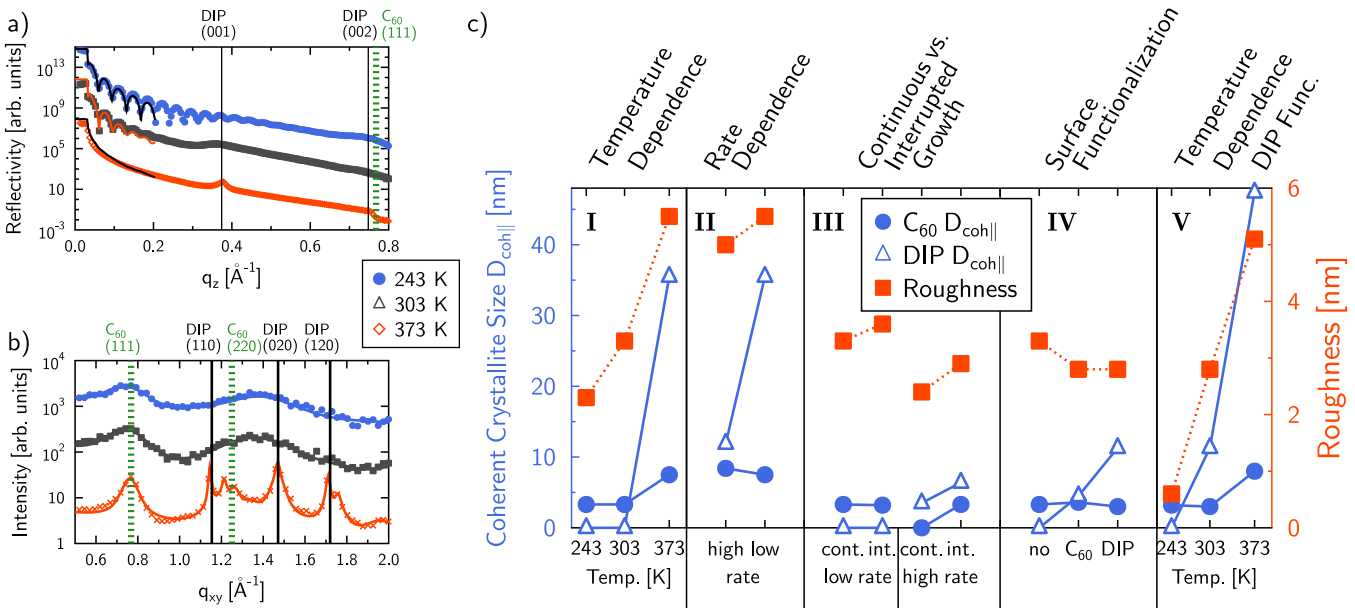

FIG. 2. (a) XRR data of DIP:C_{60} at different substrate temperatures. Solid lines are fits using Parratt's formalism. (b) GIXD data of the same mixtures. Solid lines are fits to the data. (c) Evolution of $D_{coh\|}$ and σ for different growth modifications. (**I**) Different substrate temperatures on bare nSiO. (**II**) Comparison for the high vs. low r_{dep} at $T_{sub} = 373$ K. (**III**) Normal vs. interrupted growth at low r_{dep} and high r_{dep} ($T_{sub} = 303$ K). (**IV**) Bare substrate vs. C_{60} and DIP functionalization layer at $T_{sub} = 303$ K. (**V**) Different substrate temperatures on DIP functionalization layer.

(Fig. 2(c) **V** and **IV**, respectively). For the DIP layers, σ is slightly smaller than the ones of films without a functionalization layer, at all T_{sub}. Coincidently, $D_{coh\|}$ of DIP is increased by employing a DIP layer to 11.3 nm at 303 K (where $D_{coh\|}$ cannot be determined without the DIP layer) and from 35.5 nm to 47.4 nm at $T_{sub} = 373$ K. $D_{coh\|}$ of C_{60} is not changing significantly upon employing a DIP functionalization layer, for the two higher T_{sub}. At $T_{sub} = 243$ K, $D_{coh\|}$ of DIP (cannot be determined) and C_{60} (3.3 nm), respectively, do not change when first depositing a pure DIP layer. For the C_{60} layer, the effect is similar. A small increase of $D_{coh\|}$ of DIP to 4.5 nm is observed, and $D_{coh\|}$ of C_{60} is increased from 3.3 nm to 3.6 nm. Please note that $D_{coh\|}$ of the DIP monolayer is 6.9 nm, and different from the values of the mixtures.

The different preparation conditions reported within this study have a significant impact on the growth of the DIP:C_{60} mixtures. The strongest influence, within the studied parameter space, can be associated with the T_{sub} during the growth. A higher T_{sub} implies a higher diffusion energy of the molecules and this allows molecules to rearrange on the surface to an energetically favourable position, leading to a larger length-scale of phase-separation l_s. Together with this, also a higher roughness σ is observed. Simultaneously, at a low T_{sub}, the films show a very low crystallinity, and therefore, no real phase-separation at all, yet, the films are relatively smooth. This indicates a positive correlation between l_s and σ of the films. However, it is not easy to conclude from a rougher surface a higher l_s directly, since the differences in σ are relatively low compared to the differences observed for l_s. Interestingly, no indications of lying-down DIP molecules or the low-temperature bulk crystal phase are observed at $T_{sub} = 243$ K, as is the case for pure DIP films at 233 K.[16]

It is usually the case that either a high deposition rate or a low T_{sub} should have a similar effect on the phase separation. At $T_{sub} = 373$ K, the influence of decreasing r_{dep} by a factor of ten on $D_{coh\|}$ of DIP is of the same order as increasing T_{sub} from 303 K to 373 K. Nevertheless, decreasing the deposition rate at low substrate temperatures has a significantly smaller influence on l_s than increasing T_{sub}. However, higher deposition rates lead to a smoother film surface for the investigated T_{sub}.

Interrupting the growth periodically increases the average diffusion length on the surface. In the case of a relatively low deposition rate (0.15 nm/min), interrupting the growth seems to have no influence on the structure of the mixture. Nevertheless, the controlled interruption of the growth leads to actually higher crystallinity, in the case of a high deposition rate (1.2 nm/min). The growth conditions at r_{dep}^{low} and $T_{sub} = 303$ K seem to be relatively close to equilibrium conditions, since the interruptions have no influence.

A DIP monolayer under the mixture has a strong templating effect on the film growth and improves mainly the DIP crystal structure, leading to a larger length-scale of phase separation at 303 K and 373 K. At 243 K, this effect is not observed. A C_{60} functionalization layer at $T_{sub} = 303$ K does not show an effect as pronounced as for DIP, but it is observable. Employing a functionalization layer seems to decrease the interaction potential between the substrate and the molecules, resulting in a higher diffusion length of the molecules, and therefore, in more phase separation. However, at low substrate temperatures, the effect of the low $D(T)$ due to the low T_{sub} is outweighing the benefit of a favorable surface potential.

Using mixtures with l_s lower than the exciton diffusion lengths of the materials (for DIP and C_{60} 100 nm[12] and 40 nm,[33] respectively, under ideal conditions), but still as large as possible should improve OPV cells. Our results are already close to the optimum; however, the methods presented in this work can be extended easily to increase l_s further for even better charge transport, as in the following: higher T_{sub} (with the desorption temperature as upper limit), lower r_{dep}, a specialized surface functionalization, or different preparation methods, which are closer to thermal equilibrium, e.g., organic vapor phase deposition[34] or hot wall epitaxy.[35] OPV cells with mixtures of DIP:C_{60} prepared on a thin DIP functionalization layer show domain sizes of ~90 and ~20 nm for DIP and C_{60}, respectively. For this type of cells, the short circuit current is significantly higher than for the geometry where pure C_{60} is put on pure DIP, since in the latter case probably less excitons reach the interface between the two materials to be separated.[36]

Summarizing, we have shown all the important tools to tailor the length-scale of phase separation in organic semiconductor thin film blends. The strongest impact observed was the substrate temperature. Also, the deposition rate as well as the functionalization layers can be employed to gain a similar effect, especially in cases when the substrate temperature cannot be changed.

We thank R. Jacobs, M. Oettel, and M. Klopotek for fruitful discussions. This work was supported by the German Research Foundation (DFG) within the priority program SPP 1355 "Elementary Processes of Organic Solar Cells," by the Baden-Württemberg Stiftung, and by the European Union. C.L. thanks the Carl-Zeiss-Stiftung for funding.

[1]T. Michely and J. Krug, *Islands, Mounds, and Atoms. Patterns and Processes in Crystal Growth Far from Equilibrium* (Springer, Berlin, 2004).
[2]G. Witte and C. Wöll, J. Mater. Res. **19**, 1889 (2004).
[3]S. R. Forrest, Chem. Rev. **97**, 1793 (1997).
[4]A. Pimpinelli and J. Villain, *Physics of Crystal Growth* (Cambridge University Press, Cambridge, 1998).
[5]A. Hinderhofer and F. Schreiber, ChemPhysChem **13**, 628 (2012).
[6]J. Yang, D. Yan, and T. S. Jones, Chem. Rev. **115**, 5570 (2015).
[7]A. Aufderheide, K. Broch, J. Novák, A. Hinderhofer, R. Nervo, A. Gerlach, R. Banerjee, and F. Schreiber, Phys. Rev. Lett. **109**, 156102 (2012).
[8]F. Schreiber, Phys. Status Solidi A **201**, 1037 (2004).
[9]A. Opitz, J. Wagner, W. Brütting, I. Salzmann, N. Koch, J. Manara, J. Pflaum, A. Hinderhofer, and F. Schreiber, IEEE J. Sel. Top. Quantum Electron. **16**, 1707 (2010).
[10]J. Wagner, M. Gruber, A. Hinderhofer, A. Wilke, B. Bröker, J. Frisch, P. Amsalem, A. Vollmer, A. Opitz, N. Koch, F. Schreiber, and W. Brütting, Adv. Funct. Mater. **20**, 4295 (2010).
[11]R. Banerjee, J. Novák, C. Frank, C. Lorch, A. Hinderhofer, A. Gerlach, and F. Schreiber, Phys. Rev. Lett. **110**, 185506 (2013).
[12]D. Kurrle and J. Pflaum, Appl. Phys. Lett. **92**, 133306 (2008).
[13]A. K. Tripathi and J. Pflaum, Appl. Phys. Lett. **89**, 082103 (2006).
[14]A. C. Dürr, F. Schreiber, K. A. Ritley, V. Kruppa, J. Krug, H. Dosch, and B. Struth, Phys. Rev. Lett. **90**, 016104 (2003).

[15]A. C. Dürr, F. Schreiber, M. Münch, N. Karl, B. Krause, V. Kruppa, and H. Dosch, Appl. Phys. Lett. **81**, 2276 (2002).
[16]S. Kowarik, A. Gerlach, S. Sellner, L. Cavalcanti, O. Konovalov, and F. Schreiber, Appl. Phys. A **95**, 233 (2009).
[17]A. Hinderhofer, T. Hosokai, K. Yonezawa, A. Gerlach, K. Kato, K. Broch, C. Frank, J. Novák, S. Kera, N. Ueno, and F. Schreiber, Appl. Phys. Lett. **101**, 033307 (2012).
[18]C. Frank, R. Banerjee, M. Oettel, A. Gerlach, J. Novák, G. Santoro, and F. Schreiber, Phys. Rev. B **90**, 205401 (2014).
[19]P. Peumans and S. R. Forrest, Appl. Phys. Lett. **79**, 126 (2001).
[20]H. Hoppe and N. S. Sariciftci, J. Mater. Res. **19**, 1924 (2004).
[21]M. Riede, T. Mueller, W. Tress, R. Schueppel, and K. Leo, Nanotechnology **19**, 424001 (2008).
[22]A. Hinderhofer, A. Gerlach, K. Broch, T. Hosokai, K. Yonezawa, K. Kato, S. Kera, N. Ueno, and F. Schreiber, J. Phys. Chem. C **117**, 1053 (2013).
[23]K. A. Ritley, B. Krause, F. Schreiber, and H. Dosch, Rev. Sci. Instrum. **72**, 1453 (2001).
[24]See supplementary material at http://dx.doi.org/10.1063/1.4935545 for more information on XRR, GIXD and the respective data of all films.
[25]L. G. Parratt, Phys. Rev. **95**, 359 (1954).
[26]M. Björck and G. Andersson, J. Appl. Crystallogr. **40**, 1174 (2007).
[27]P. Scherrer, Nachr. Ges. Wiss. Göttingen, Math-Phys Kl. **1918**, 98 (1918), available at https://eudml.org/doc/59018.
[28]S. Schinzer, M. Sokolowski, M. Biehl, and W. Kinzel, Phys. Rev. B **60**, 2893 (1999).
[29]T. Wagner, D. R. Fritz, and P. Zeppenfeld, Org. Electron. **12**, 442 (2011).
[30]J. L. de Boer, S. van Smaalen, V. Petricek, M. Dusek, M. A. Verheijen, and G. Meijer, Chem. Phys. Lett. **219**, 469 (1994).
[31]H. Kiessig, Ann. Phys. **402**, 769 (1931).
[32]A. C. Dürr, N. Koch, M. Kelsch, A. Rühm, J. Ghijsen, R. L. Johnson, J.-J. Pireaux, J. Schwartz, F. Schreiber, H. Dosch, and A. Kahn, Phys. Rev. B **68**, 115428 (2003).
[33]P. Peumans, A. Yakimov, and S. R. Forrest, J. Appl. Phys. **93**, 3693 (2003).
[34]M. Baldo, M. Deutsch, P. Burrows, H. Gossenberger, M. Gerstenberg, V. Ban, and S. Forrest, Adv. Mater. **10**, 1505 (1998).
[35]A. Lopez-Otero, Thin Solid Films **49**, 3 (1978).
[36]M. Gruber, M. Rawolle, J. Wagner, D. Magerl, U. Hörmann, J. Perlich, S. V. Roth, A. Opitz, F. Schreiber, P. Müller-Buschbaum, and W. Brütting, Adv. Energy Mater. **3**, 1075 (2013).